THE JOURNAL OF PHYSICAL CHEMISTRY C

Article

pubs.acs.org/JPCC

Orientation Dependence of Plasmonically Enhanced Spontaneous Emission

T. V. Raziman and Olivier J. F. Martin*

Nanophotonics and Metrology Laboratory (NAM), Swiss Federal Institute of Technology Lausanne (EPFL), 1015 Lausanne, Switzerland

Supporting Information

ABSTRACT: We computationally explore how the orientation of dipolar emitters placed near plasmonic nanostructures affects their radiative enhancement and spontaneous emission rate. We demonstrate that the expressions for these quantities show a subtle dependence on the molecular orientation, and this information is lost when typical calculations assume a random orientation and perform an average over all directions. This orientation dependence is strongly affected by the location of the emitter, the emission wavelength, and the symmetry of the system. While the plasmonic nanostructure can significantly modify the far-field from a molecule in its vicinity, this modification is heavily dependent on both the wavelength and the orientation of the emitter. We show that if a fluorescent molecule can be constrained to emit in a specific direction, we are able to obtain far superior control over its spontaneous emission and decay rate than otherwise and discuss implications for single molecule experiments.

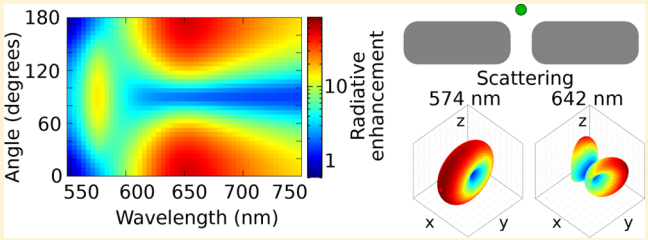

INTRODUCTION

Resonant plasmonic structures provide extreme confinement and enhancement of electromagnetic fields upon external illumination.[1−6] They also have the ability to boost the radiation from emitters placed nearby. In combination, these effects make plasmonic systems ideal for enhancing weak processes such as fluorescence[7−17] and Raman scattering.[18−27] Plasmonic chemical and biological sensors based on these processes have found wide application, and it is possible to detect even single molecules in this fashion.[28−32]

The increase in radiation from emitters such as excited fluorescent molecules placed near plasmonic nanostructures is due to the enhancement of their spontaneous emission rate (SPER), which arises from the increase in the local density of states (LDOS).[33] This phenomenon is known as the Purcell effect.[34] However, though the spontaneous emission rate is enhanced, it is not entirely transmitted to the far-field due to plasmonic quenching whereby the nanostructure absorbs a fraction of the emitted photons.[10,35,36] SPER and radiative enhancements and plasmonic quenching can be computed using classical electromagnetic theory.[13,37−40] Manipulating the spontaneous emission from emitters has a lot of practical applications, and this has been achieved through the use of photonic crystals, nanocavities, and metamaterials.[41−45]

The orientation of the excited molecules has a strong influence on spontaneous emission. However, fluorescent molecules are usually assumed to be randomly oriented, and plasmonic calculations are performed by averaging over all possible orientations.[15,46] Some studies have done a basic treatment of orientation dependence by considering dipoles oriented in cardinal directions such as along various axes of nanostructures and normal to the nanostructure surfaces[12,39,47−50] or located at symmetry points of the nanostructure.[51,52] All these assumptions result in suppressing some aspects of the orientation dependence of spontaneous emission. In this article, we go beyond these assumptions and perform a comprehensive computational study on how the orientation of emitters placed near plasmonic antennae affects their SPER and radiative enhancement. We look at how the nonlinear nature of the expressions describing the emission results in a rich dependence on orientation and numerically demonstrate this effect on emitters placed near plasmonic gap antennae and V-shaped antennae. We show that the orientation corresponding to maximum SPER and radiative enhancements is strongly affected by the location of the emitter, symmetry breaking, and the wavelength and also investigate how this is transmitted to the far-field. To the best of our knowledge, this is the first comprehensive study on the orientation dependence of plasmonically enhanced spontaneous emission that deals with all these aspects.

THEORY AND METHOD

The computations in this article are performed using the surface integral equation (SIE) formulation.[53] Since it is required to simulate strongly varying fields and structures in close proximity, a high accuracy SIE implementation is used.[54] All the simulations are performed with vacuum as the

Special Issue: Richard P. Van Duyne Festschrift

Received: April 4, 2016
Revised: June 2, 2016
Published: June 2, 2016

DOI: 10.1021/acs.jpcc.6b03297
J. Phys. Chem. C 2016, 120, 21037−21046

background, and the nanostructures are modeled to be made out of gold with permittivity given by the Drude formula,

$$\tilde{\epsilon}(\omega) = \epsilon_\infty - \frac{{\omega_p}^2}{\omega(\omega + i\gamma)} \tag{1}$$

with Drude parameters $\epsilon_\infty = 9.5$, $\omega_p = 8.95$ eV, and $\gamma = 0.0691$ eV to fit the permittivity data from Johnson and Christy.[55−57] This model neglects the increased absorption for gold at low wavelengths (<650 nm) and was chosen to have a smooth variation of permittivity so that we can focus on the basic physics instead of the absorptive behavior specific to gold. Care must hence be taken while comparing the numerical results at low wavelengths with experimental findings.

The emitter can be modeled as a dipole oscillating at a frequency ω. For a dipole located at $\mathbf{r}$ oscillating in the direction $\hat{\mathbf{n}}$, the SPER enhancement F_{SPER} due to the presence of a plasmonic nanostructure can be computed using[46,58]

$$F_{SPER} = \frac{\hat{\mathbf{n}}\cdot \mathrm{Im}[\bar{\mathbf{G}}(\mathbf{r},\mathbf{r})]\cdot\hat{\mathbf{n}}}{k/(6\pi)} \tag{2}$$

where $\bar{\mathbf{G}}$ is the dyadic Green's function[59] and $k = \omega/c$ is the wavenumber. It can be immediately seen that the F_{SPER} operator is nonlinear in $\hat{\mathbf{n}}$; knowing the values of F_{SPER} for two orientations of the dipole does not immediately give us the value of F_{SPER} for a linear combination of them. For example, we have for dipoles oriented along $\hat{x}$ and $\hat{y}$, $F_{SPER}(\hat{x}) = \mathrm{Im}[G_{xx}]/[k/(6\pi)]$ and $F_{SPER}(\hat{y}) = \mathrm{Im}[G_{yy}]/[k/(6\pi)]$. However, for an arbitrary dipole in the xy-plane oriented at an angle θ from the x-axis, we have

$$F_{SPER}(\hat{x}\cos\theta + \hat{y}\sin\theta) = \frac{\mathrm{Im}[G_{xx}\cos^2\theta + (G_{xy} + G_{yx})\sin\theta\cos\theta + G_{yy}\sin^2\theta]}{k/(6\pi)} \tag{3}$$

Off-diagonal terms of the Green's tensor appear, resulting in an interesting orientation dependence. In the absence of the off-diagonal terms, the function in eq 3 would have had its extrema at $\theta = 0$ and $\pi/2$. However, with the inclusion of these terms the extrema of the function could be at any angle. This argument extends to dipoles oriented arbitrarily in three dimensions naturally. We will explore the consequences of this orientation dependence in this paper. If the emitter is assumed to have a random orientation and we average over all possible orientations, we have

$$\langle F_{SPER}\rangle = \frac{\mathrm{Im}\{\mathrm{Tr}[\bar{\mathbf{G}}(\mathbf{r},\mathbf{r})]\}}{k/(2\pi)} \tag{4}$$

where $\langle\ldots\rangle$ denotes averaging over orientations and Tr denotes taking the trace. That is, once the averaging is done, the off-diagonal terms in the tensor do not contribute to the SPER. It is thus necessary to constrain the dipole orientation in order to be able to notice the orientation effects. Although many experiments on molecules interacting with plasmonic nanostructures are performed in liquid, where the molecules can rotate freely, it is also possible to control the conformation between molecule and nanostructure to favor specific orientations.[60−62] Actually, even the rotation speed of molecules near plasmonic nanostructures can influence the fluorescence emission and can be used to measure locally the temperature.[63,64]

The radiative enhancement F_{rad} due to the nanostructure can be computed by finding the total (incident + scattered) field on a sphere S enclosing the nanostructure and the dipole, integrating the Poynting vector on it, and normalizing it to the field in the absence of the nanostructure,[65]

$$F_{rad} = \frac{\oint_S \frac{1}{2}\mathrm{Re}[\mathbf{E}_{tot}\times\mathbf{H}^*_{tot}]\cdot\hat{\mathbf{n}}_S\,dS}{\oint_S \frac{1}{2}\mathrm{Re}[\mathbf{E}_{inc}\times\mathbf{H}^*_{inc}]\cdot\hat{\mathbf{n}}_S\,dS} \tag{5}$$

where $\mathbf{E}$ and $\mathbf{H}$ are the electric and magnetic fields, respectively, $\hat{\mathbf{n}}_S$ is the outward normal to the surface, and the subscripts tot and inc correspond to total and incident fields, respectively. It should be noted that the denominator is independent of the orientation of the dipole and is equal to the total radiation emitted by a dipole in free space,[66]

$$P_{dip} = \frac{\omega^4\mu_0}{12\pi c}|\mathbf{p}|^2 \tag{6}$$

where μ_0 is the permeability of free space, c is the speed of light, and $\mathbf{p}$ is the dipole moment. F_{rad} shows the same nonlinear nature as F_{SPER}. For example, if dipoles oriented along $\hat{x}$ and $\hat{y}$ result in fields $\{\mathbf{E}^x,\mathbf{H}^x\}$ and $\{\mathbf{E}^y,\mathbf{H}^y\}$, respectively, cross terms like $\mathbf{E}^x\times\mathbf{H}^{y*}$ appear in F_{rad} for other orientations. These cross terms arising due to the interaction between the fields are perhaps more intuitive to understand than the cross terms in F_{SPER}. However, the mathematical form and behavior of the cross terms in the two cases are identical. If we average over all possible orientations of the dipole, the cross terms in F_{rad} disappear as well.

In the same fashion, by integrating the Poynting vector around the nanostructure surface S_p and normalizing it to the free space dipole radiation, we obtain the nonradiative enhancement due to the absorption F_{nr},

$$F_{nr} = -\frac{\oint_{S_p}\frac{1}{2}\mathrm{Re}[\mathbf{E}_{tot}\times\mathbf{H}^*_{tot}]\cdot\hat{\mathbf{n}}_p\,dS_p}{P_{dip}} \tag{7}$$

However, this method of calculating the absorption often results in numerical errors, and an alternative method can be employed using the ohmic loss in the metal,[65]

$$F_{nr} = \frac{\int_{V_p}\frac{1}{2}\mathrm{Re}\{\sigma\}|\mathbf{E}_{tot}|^2\,dV_p}{P_{dip}} \tag{8}$$

where V_p is the volume of the nanostructure and σ the conductivity. The integration is typically performed using a Monte Carlo method to choose points randomly inside the nanostructure volume. F_{nr} has similar behavior as F_{rad}, with cross terms resulting in nonlinearity of the operator. The total energy lost by the dipole should be equal to the sum of energy radiated into the far-field and lost into the plasmonic nanostructures; hence we expect $F_{SPER} = F_{rad} + F_{nr}$.

Note that in addition to the factors discussed here, the overall emission of a molecule coupled to a plasmonic nanostructure is also affected by the plasmonic enhancement of incident local field. We do not consider that effect here for simplicity, and we concern ourselves only with the spontaneous emission rate and radiative enhancement. The spontaneous emission rate is what affects the measurement of fluorescence lifetimes, and radiative enhancement is the dominant factor influencing fluorescence in the case of good emitters upon strong illumination.[13]

DOI: 10.1021/acs.jpcc.6b03297
J. Phys. Chem. C 2016, 120, 21037−21046

RESULTS AND DISCUSSION

Gap Antenna. The first system we consider is a symmetric gap antenna, which has become one of the iconic systems for plasmonic molecular enhancement because of its strong tunability.[67] The antenna arms have dimensions 120 nm × 40 nm × 40 nm and are separated by a gap of 20 nm. The radiative, nonradiative, and SPER enhancements for a dipole emitter at the center of the gap oscillating along the antenna axis are shown in Figure 1 as a function of wavelength. The schematic of the antenna is shown in Figure 2a, where the current location is denoted by the blue dot. The nonradiative enhancement curve calculated using the Monte Carlo method, eq 8, is virtually identical to that computed from the surface integral of the Poynting vector, eq 7. Also, adding the radiative enhancement computed by integrating the scattered Poynting vector in the far-field, eq 5, to the nonradiative enhancement due to the absorption reproduces the SPER enhancement curve computed from the Green's tensor, eq 2. These matches provide evidence of the consistency of the numerical method, which is a consequence of the highly accurate routine used for computation.[54] Having shown that the results match, we will use SPER enhancement computed from the Green's tensor in the rest of the article.

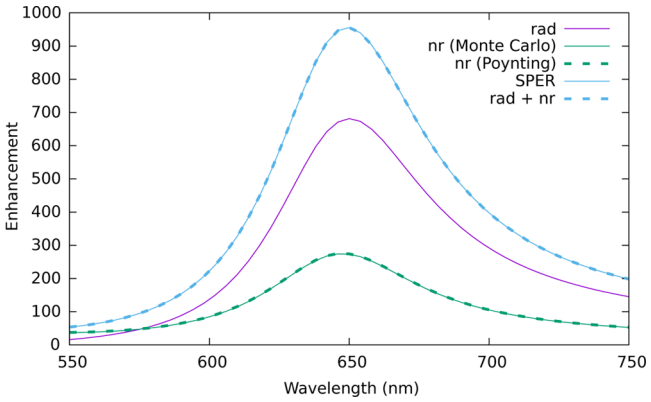

Figure 1. Radiative (rad), nonradiative (nr), and spontaneous emission rate (SPER) enhancements as a function of wavelength for a dipole polarized along x at the center of the gap antenna shown in Figure 2a. Two different techniques are used to compute the absorption for the nonradiative enhancement: Monte Carlo integration using eq 8 and integration of the Poynting vector following eq 7.

We now move on to study the orientation dependence of radiative and SPER enhancement. These quantities are plotted in Figure 2b as a function of wavelength and angle with respect to x-axis for the dipole in the gap center. Note that the dipole oscillation direction remains in the xy-plane. The radiative and SPER enhancement curves look similar except for the latter showing higher values. This is because the SPER enhancement includes the absorption in addition to the scattering, as explained previously. There is a single peak visible near $\lambda = 650$ nm, and the maximum values for SPER and radiative enhancement are found for the dipole oscillating about the x-axis ($\theta = 0$). The dipole in the gap couples most efficiently to the antenna when it oscillates along the antenna axis. The plots show vertical flip symmetry, a consequence of the horizontal symmetry of the system.

When the dipole is moved perpendicular to the antenna axis by 30 nm (green dot in Figure 2a), the resultant enhancement

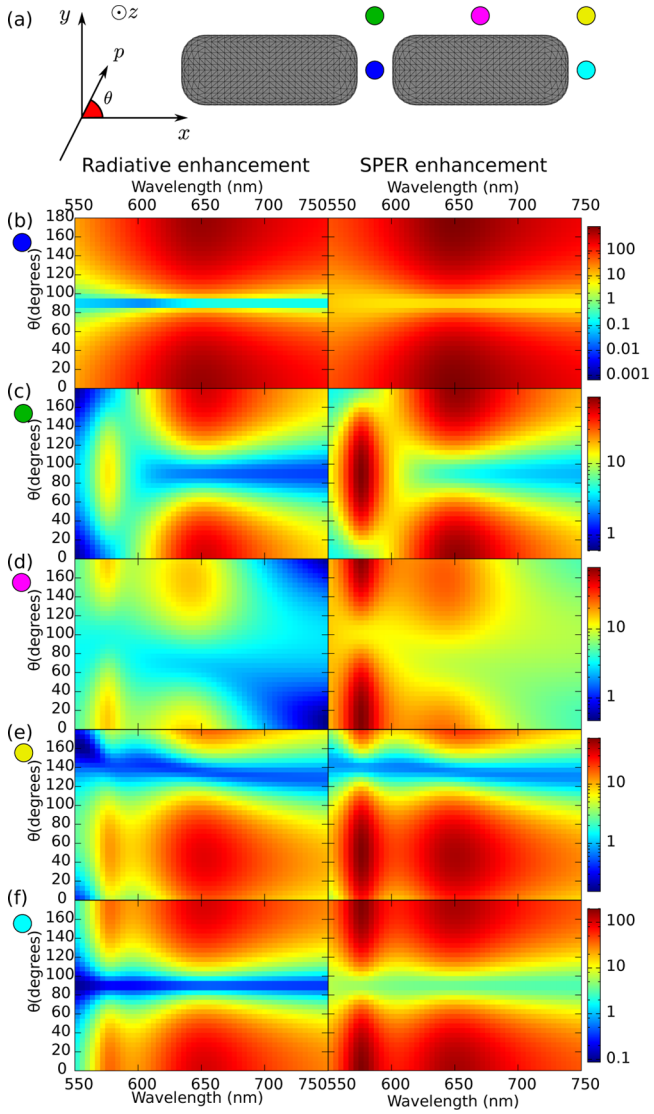

Figure 2. (a) Schematic of the gap antenna system. (b–f) Radiative enhancement (left) and SPER enhancement (right) as a function of wavelength and orientation angle for five different locations near the gap antenna marked with colored dots in (a). Note the different color scales for each panel.

plots shown in Figure 2c are quite different. The most notable feature is that a second peak has now appeared near $\lambda = 575$ nm. Near this peak, radiative and SPER enhancements are maximized for a dipole oscillating perpendicular to the antenna axis, unlike the situation for the higher wavelength peak. Even though the dipole is still quite close to the antenna, coupling with the antenna is more efficient for the dipole perpendicular to the antenna axis than parallel to it. It is also seen that throughout the wavelength range including the region between the two scattering peaks, the scattering maximum is always along one of the directions x or y. This results from the symmetry of the antenna–dipole system. As long as the dipole is placed anywhere along one of the symmetry axes of the gap antenna, the off-diagonal terms in the Green's tensor vanish. Consequently, the radiative/SPER maximum orientation will be along x or y, as seen from eq 3. The vertical flip symmetry in the plots is retained as well.

Breaking the symmetry changes the situation tremendously. When the dipole is placed 10 nm away from the center of one

DOI: 10.1021/acs.jpcc.6b03297
J. Phys. Chem. C 2016, 120, 21037–21046

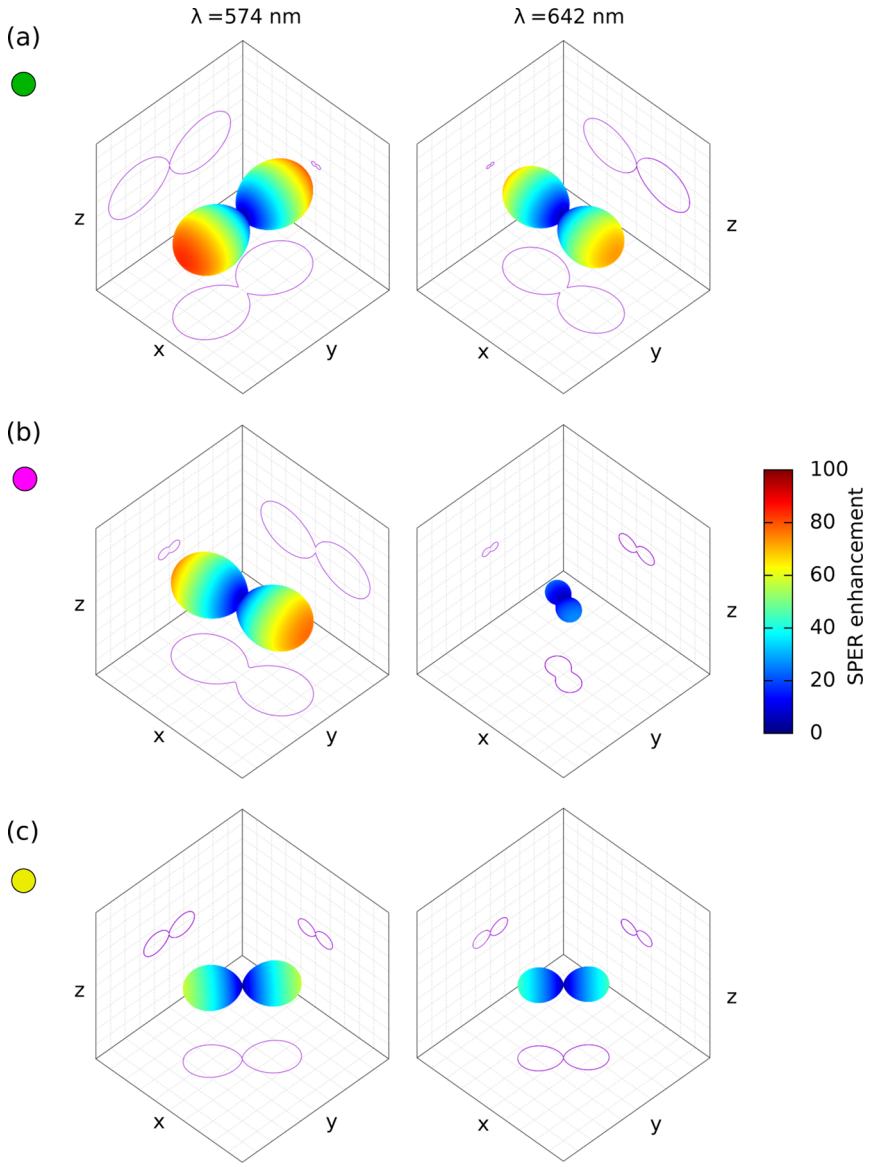

Figure 3. SPER enhancement as a function of three-dimensional orientation of the dipole at λ = 574 nm (left) and 642 nm (right) for three locations near the gap antenna marked with colored dots in Figure 2a.

of the antenna arms (magenta dot in Figure 2a), the radiative and SPER enhancement plots shown in Figure 2d are no longer flip symmetric. Two peaks appear at roughly the same wavelengths as before, but the orientations corresponding to the maxima are now different. The maxima are now seen to appear at any angle, not necessarily along *x* or *y*, which changes as a function of wavelength. The off-diagonal terms in the Green's tensor are nonzero in this case, and that is what allows the enhancement to peak at a different angle. This result shows that emitters placed in arbitrary (nonsymmetric) locations emit preferentially at orientations dependent on wavelength and different from the symmetry axes of the system. Approximating the dominant response of the dipole as being along the antenna axis or perpendicular to the antenna surface can be grossly inaccurate. Since fluorescent decay times are inversely proportional to the SPER enhancement, this orientation dependence influences the decay time measurement as well. In particular, if a fluorescent molecule can be constrained to emit in a specific orientation, we would be able to obtain far superior control over its spontaneous emission and decay rate than otherwise.

When the emitter is moved to the corner of the antenna (yellow dot in Figure 2a), the plots in Figure 2e show similar asymmetry and maxima at intermediate angles. But when we move it to the outer face of the antenna (cyan dot in Figure 2a), we return to one of the symmetry axes and, consequently, the plots in Figure 2f are symmetric again.

We now look at what happens when the dipole is allowed to rotate freely in three dimensions, that is, not restricted to the *xy*-plane. SPER enhancement as a function of orientation is shown in Figure 3 at two different wavelengths (λ = 574 and 642 nm, corresponding to the two peaks seen in Figure 2) for three locations of the dipole. SPER enhancement is plotted as a polar surface, with the distance of the surface from the origin being proportional to the SPER enhancement for that orientation. Additionally, SPER enhancement curves for orientations fixed along the cardinal planes are shown on the respective planes. For a dipole displaced from the center of the gap (green dot in Figure 2a), the resultant surface in Figure 3a is dumbbell-shaped. It should be noted that the surface is not exactly cylindrically symmetric about the axis: the SPER

DOI: 10.1021/acs.jpcc.6b03297
J. Phys. Chem. C 2016, 120, 21037−21046

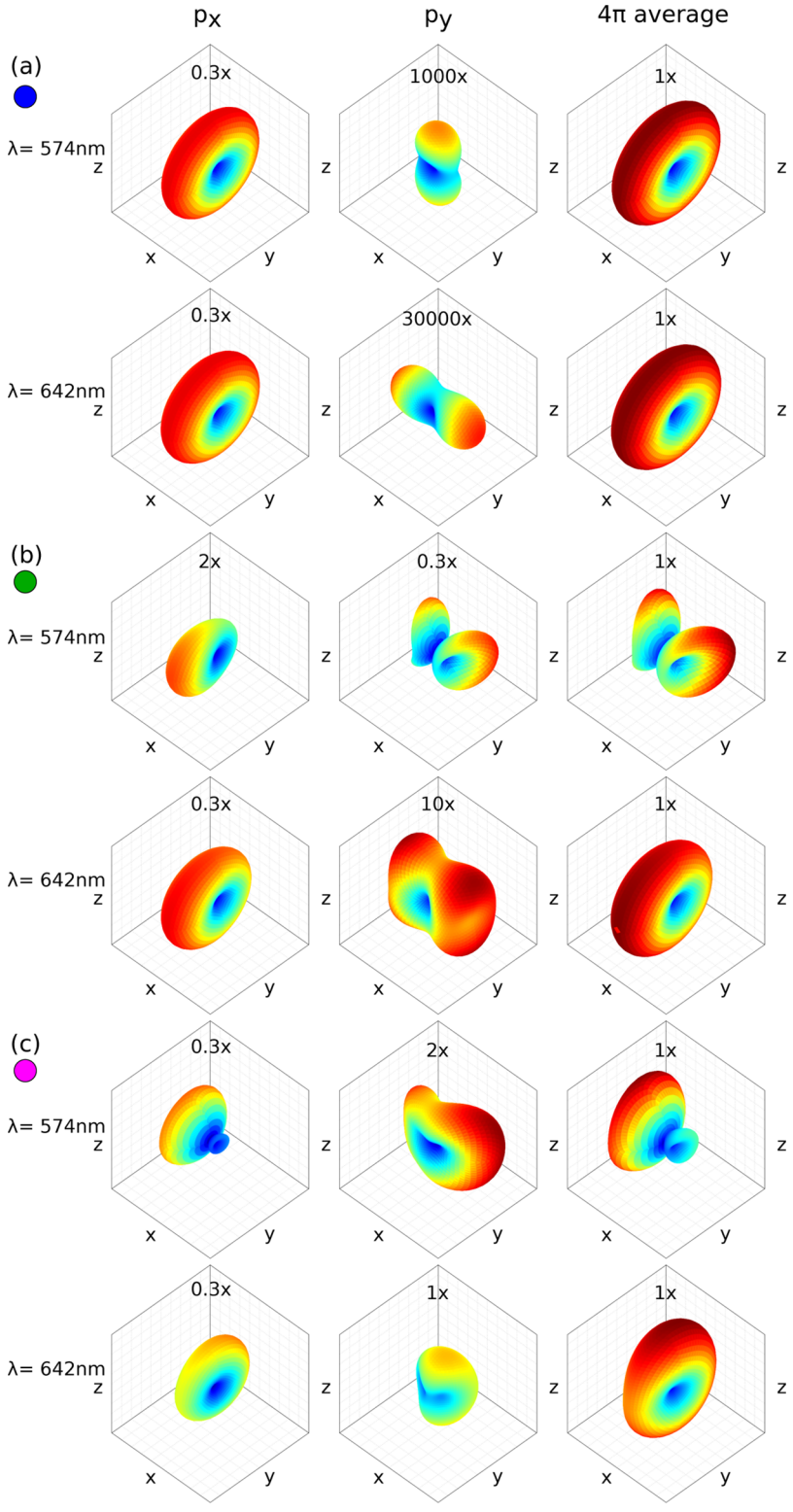

Figure 4. Normalized three-dimensional scattering patterns at λ = 574 and 642 nm for dipoles located at three positions near the gap antenna marked with colored dots in Figure 2a, for *x*-polarization (left), for *y*-polarization (center), and averaged over all orientations of the dipole (right).

enhancement along *z*-axis is much smaller than that along the other two axes; response of the dipole perpendicular to the nanostructure plane can thus be mostly neglected. The axis of the dumbbell changes from *y* to *x* on going from lower wavelength to higher wavelength, following the behavior seen in Figure 2c. However, it should be noted that the axis of the dumbbell does not rotate continuously (this would imply that the SPER maximum happens at a different angle at an intermediate wavelength, which is symmetry-forbidden as discussed previously) but evolves through stretching and compression of the dumbbell, as clear from the wavelength evolution shown in video V1 (Supporting Information). On breaking the symmetry by moving to a different location near the center of one of the arms, the dumbbell axis can be in a

DOI: 10.1021/acs.jpcc.6b03297
J. Phys. Chem. C 2016, 120, 21037−21046

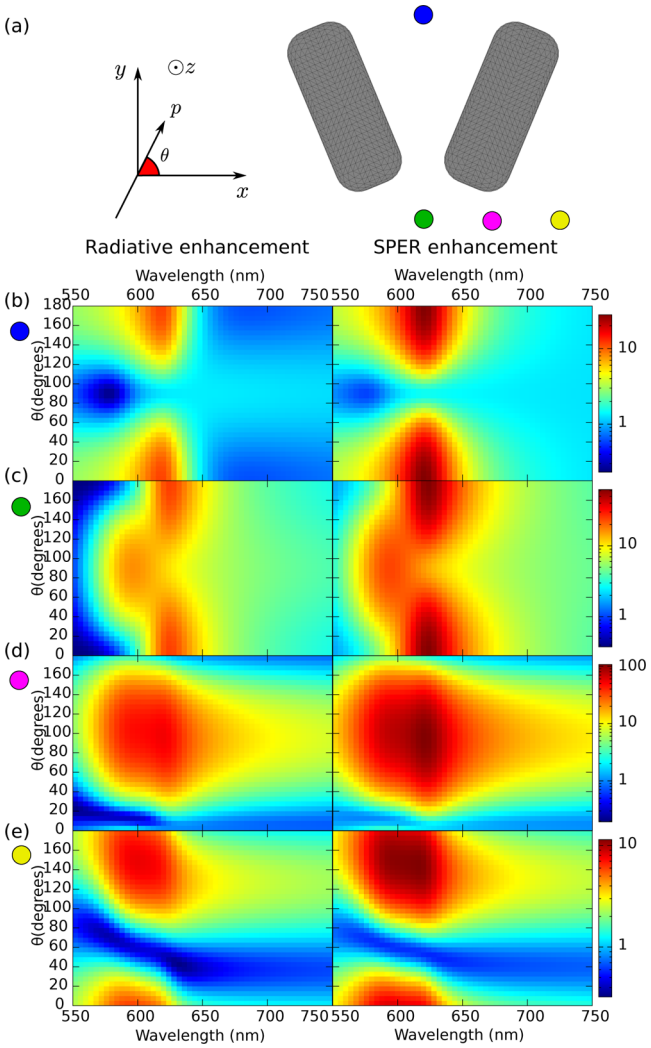

Figure 5. (a) Schematic of the V-shaped antenna. (b–e) Radiative enhancement (left) and SPER enhancement (right) as a function of wavelength and orientation angle for four different locations marked with colored dots in (a).

different direction as seen in Figure 3b. Continuous rotation of the axis is also possible in this situation as seen in the wavelength evolution in video V2 (Supporting Information). Similar behavior is seen for the dipole located near the corner, Figure 3c and video V3 (Supporting Information).

A common feature of all these plots is that the SPER enhancement varies significantly as a function of orientation, by orders of magnitude. If the molecules are distributed in a randomly oriented fashion, the resultant average SPER enhancement is merely an average over all orientations, and this large range of SPERs is lost. Being able to fix the orientations of molecules would thus provide tremendous control over spontaneous emission rates and decay times.

Plasmonic nanostructures have been used to obtain directionality for fluorescent and Raman emission,[68−72] and this directionality has been shown to be dependent on the orientation of the emitter.[73,74] We will now study this effect for the gap antenna, looking at the how the orientation of the emitter affects its far-field radiation pattern.

The normalized far-field scattering pattern is plotted for three locations of the emitter at two wavelengths (λ = 574 and 642 nm) in Figure 4. Three plots are shown for each location−wavelength pair: far-field scattering pattern for an emitter polarized along x (p_x), for one polarized along y (p_y), and the average taken over all possible orientations (4π average). It should be noted that the plots for p_x and p_y have been multiplied by different factors to make them comparable to the 4π average. Also, since the normalization for each set set corresponding to a location−wavelength pair has been done with respect to the 4π average plot in the set, magnitudes of the plots in different sets cannot be compared.

When the emitter is placed at the center of the gap and polarized along x, the radiation is donut shaped, see Figure 4a. This is the expected radiation pattern for a dipole.[66] However, when the emitter is polarized along y, the radiation is maximally along z- and x-directions at λ = 574 and 642 nm, respectively. The antenna thus strongly modifies the far-field from the emitter, and this modification is heavily dependent on both the wavelength and the orientation of the emitter. It is also evident that the radiation for the x-polarized emitter is orders of magnitude stronger than for the y-polarized one. Since x-polarized emitters in the gap couple maximally efficiently with the antenna, averaging over all orientations results in a shape which follows that polarization. The symmetry of the system and the location results in inversion symmetry of the scattering pattern about all axes.

However, this symmetry is broken when we displace the emitter outside the gap, Figure 4b. The scattering in this case is qualitatively different from that of the emitter in the center, and there is strong forward/backward dominance of the scattering depending on the orientation and wavelength. Also, it is the y-polarized emitter that dominates in the far-field at λ = 574 nm, as expected from the orientation dependence of radiative enhancement observed previously in Figure 2c. When the emitter is moved away from the symmetry axis, Figure 4c, the radiation patterns become even further asymmetric.

These results show that it is extremely important to consider the orientation dependence of emission while measuring plasmonically enhanced fluorescence. As the wavelength is varied, the orientation of the emitter that gives maximum scattering can change, modifying the far-field pattern. Unless the fluorescence measurement incorporates this variation, one would end up with a misleading spectrum, especially if the measurement is done with a detector along one of the cardinal directions with a small collection angle.

Finally, we note that as a result of electromagnetic reciprocity, the scattering patterns computed here are related to excitation enhancements due to incident illuminations.[39,75,76] Plane waves incident from different directions excite dipoles of different orientations differently, and these excitation enhancements are proportional to the scattering for the respectively oriented dipoles in those directions. By application of electromagnetic reciprocity, the results in Figure 4 hence imply that the orientation of the dipole strongly affects not only its spontaneous emission and radiative enhancements but also how well it can be excited by incident illumination. The orientation dependence of total fluorescent or Raman response is a combination of the excitation and emission responses. Additionally, in the case of Raman scattering, we need to take into account the coupling between excitation and emission orientations, which is dependent on the molecular symmetries and expressed via surface selection rules.[24,77] The resulting polarization dependence of plasmonically enhanced Raman scattering has been experimentally verified.[51,78] However, it should be noted that these studies consider the orientation only

DOI: 10.1021/acs.jpcc.6b03297
J. Phys. Chem. C 2016, 120, 21037−21046

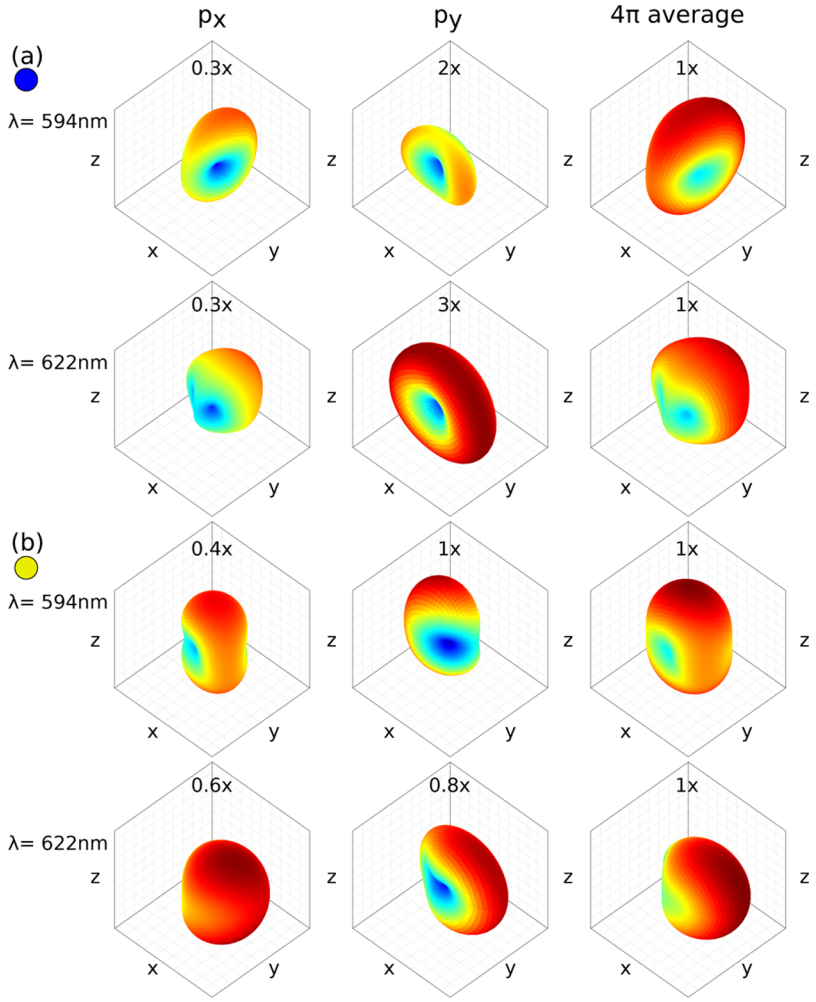

Figure 6. Three dimensional scattering patterns at λ = 594 and 622 nm for dipoles located at two positions near the V-shaped antenna marked with colored dots in Figure 5a, for *x*-polarization (left), for *y*-polarization (center), and averaged over all orientations of the dipole (right).

indirectly through the incident and scattered polarizations and not through direct constrainment of emitter orientation.

V-Shaped Antenna. Next, we break the symmetry of the gap antenna and remove the point of inversion by changing the angle between the arms to 45°, as shown in the schematic of Figure 5a. The resultant V-shaped antenna has only one symmetry axis in the *xy*-plane. This type of plasmonic antenna has been used to build metasurfaces that manipulate the phase of incoming light.[79]

When the dipole is placed on the symmetry axis (Figure 5b,c, corresponding to blue and green dots in Figure 5a), we once again have the situation that radiative and SPER maxima are along *x*- or *y*-axis for all wavelengths. On the contrary, when the emitter is placed away from the symmetry axis (Figure 5d,e, corresponding to magenta and yellow dots in Figure 5a), we have asymmetric enhancement with peak enhancement angle continuously varying as a function of wavelength. These observations are consistent with the discussion in the previous section about the gap antenna.

Finally, we look at the far-field radiation pattern from the antenna in Figure 6. Since the V-shaped antenna does not have any point of inversion, we do not obtain symmetric radiation patterns in any case. When the emitter is placed on the symmetry axis (Figure 6a, corresponding to the blue dot in Figure 5a), the radiation pattern is symmetric about the axis as well. When the emitter is polarized along *x*, most of the radiation is directed in the +*y*-direction by the antenna. When the emitter is polarized along *y*, the peak scattering is in the *xz*-plane. Due to the relatively more efficient coupling, it is the signature of the *x*-polarized emitter that is prominent when all possible orientations are averaged. The radiation patterns for the two wavelengths show significant differences as well. When the emitter is placed away from the symmetry axis (Figure 6b, corresponding to the yellow dot in Figure 5a), the radiation pattern is no longer symmetric. The qualitative features are also quite different, and the direction in which most of the radiation is emitted can be quite different from the cardinal directions. This is most clearly visible on averaging the scattering from all possible orientations of the emitter at λ = 622 nm. In systems such as the V-shaped antenna where the symmetry is broken, the orientation dependence becomes even more significant than otherwise.

■ CONCLUSION

We have shown how the nonlinear operators corresponding to radiative and SPER enhancement give rise to a complex orientation dependence for these quantities in the presence of plasmonic nanostructures. Depending on the location of the emitter and the wavelength of emission, the orientation resulting in maximum enhancement can vary significantly,

DOI: 10.1021/acs.jpcc.6b03297
J. Phys. Chem. C 2016, 120, 21037−21046

especially if symmetry is broken in the system. By controlling the orientation of emitters, it is possible to achieve superior control over spontaneous emission. The orientation dependence of scattering affects the far-field radiation pattern as well. Hence these effects should be properly accounted for in theoretical calculations as well as while designing experiments involving plasmonic fluorescence enhancement. In particular, care must be taken to ensure that the equipment used to detect fluorescent signal is positioned properly to account for the changes in the far-field scattering pattern as a function of position and orientation of emitters.

■ ASSOCIATED CONTENT

Supporting Information

The Supporting Information is available free of charge on the ACS Publications website at DOI: 10.1021/acs.jpcc.6b03297.

Video V1: three dimensional orientation dependence of SPER enhancement as a function of wavelength for a dipole displaced from the center of the gap of the gap antenna in a direction perpendicular to the axis of the antenna (green dot in Figure 2a) (AVI)

Video V2: Three dimensional orientation dependence of SPER enhancement as a function of wavelength for a dipole placed near the center of one of the arms of the gap antenna (magenta dot in Figure 2a) (AVI)

Video V3: Three dimensional orientation dependence of SPER enhancement as a function of wavelength for a dipole placed near the outer corner of a gap antenna (yellow dot in Figure 2a) (AVI)

■ AUTHOR INFORMATION

Corresponding Author

*E-mail: olivier.martin@epfl.ch. Phone: +41-21-693-26-07.

Notes

The authors declare no competing financial interest.

■ ACKNOWLEDGMENTS

The authors acknowledge funding from the Swiss National Science Foundation (Project 200020135452).

■ REFERENCES

(1) Haes, A. J.; Zou, S.; Schatz, G. C.; Van Duyne, R. P. Nanoscale Optical Biosensor: Short Range Distance Dependence of the Localized Surface Plasmon Resonance of Noble Metal Nanoparticles. *J. Phys. Chem. B* **2004**, *108*, 6961−6968.

(2) Pieczonka, N. P. W.; Aroca, R. F. Single Molecule Analysis by Surfaced-Enhanced Raman Scattering. *Chem. Soc. Rev.* **2008**, *37*, 946−954.

(3) Zhang, W.; Huang, L.; Santschi, C.; Martin, O. J. F. Trapping and Sensing 10 nm Metal Nanoparticles Using Plasmonic Dipole Antennas. *Nano Lett.* **2010**, *10*, 1006−1011.

(4) Stockman, M. I. Nanoplasmonics: Past, Present, and Glimpse into Future. *Opt. Express* **2011**, *19*, 22029−22106.

(5) Kottmann, J. P.; Martin, O. J. F.; Smith, D. R.; Schultz, S. Dramatic Localized Electromagnetic Enhancement in Plasmon Resonant Nanowires. *Chem. Phys. Lett.* **2001**, *341*, 1−6.

(6) Schlücker, S. Surface-Enhanced Raman Spectroscopy: Concepts and Chemical Applications. *Angew. Chem., Int. Ed.* **2014**, *53*, 4756−4795.

(7) Liebermann, T.; Knoll, W. Surface-Plasmon Field-Enhanced Fluorescence Spectroscopy. *Colloids Surf., A* **2000**, *171*, 115−130.

(8) Neumann, T.; Johansson, M.-L.; Kambhampati, D.; Knoll, W. Surface-Plasmon Fluorescence Spectroscopy. *Adv. Funct. Mater.* **2002**, *12*, 575−586.

(9) Yu, F.; Persson, B.; LöfÅs, S.; Knoll, W. Attomolar Sensitivity in Bioassays Based on Surface Plasmon Fluorescence Spectroscopy. *J. Am. Chem. Soc.* **2004**, *126*, 8902−8903.

(10) Lakowicz, J. R. Radiative Decay Engineering 5: Metal-Enhanced Fluorescence and Plasmon Emission. *Anal. Biochem.* **2005**, *337*, 171−194.

(11) Tam, F.; Goodrich, G. P.; Johnson, B. R.; Halas, N. J. Plasmonic Enhancement of Molecular Fluorescence. *Nano Lett.* **2007**, *7*, 496−501.

(12) Colas des Francs, G.; Bouhelier, A.; Finot, E.; Weeber, J. C.; Dereux, A.; Girard, C.; Dujardin, E. Fluorescence Relaxation in the Near-Field of a Mesoscopic Metallic Particle: Distance Dependence and Role of Plasmon Modes. *Opt. Express* **2008**, *16*, 17654−17666.

(13) Kern, A. M.; Meixner, A. J.; Martin, O. J. F. Molecule-Dependent Plasmonic Enhancement of Fluorescence and Raman Scattering near Realistic Nanostructures. *ACS Nano* **2012**, *6*, 9828−9836.

(14) Ming, T.; Chen, H.; Jiang, R.; Li, Q.; Wang, J. Plasmon-Controlled Fluorescence: Beyond the Intensity Enhancement. *J. Phys. Chem. Lett.* **2012**, *3*, 191−202.

(15) Derom, S.; Berthelot, A.; Pillonnet, A.; Benamara, O.; Jurdyc, A. M.; Girard, C.; Colas des Francs, G. Metal Enhanced Fluorescence in Rare Earth Doped Plasmonic Core-Shell Nanoparticles. *Nanotechnology* **2013**, *24*, 495704.

(16) Lu, G.; Liu, J.; Zhang, T.; Shen, H.; Perriat, P.; Martini, M.; Tillement, O.; Gu, Y.; He, Y.; Wang, Y.; et al. Enhancing Molecule Fluorescence with Asymmetrical Plasmonic Antennas. *Nanoscale* **2013**, *5*, 6545−6551.

(17) Bauch, M.; Toma, K.; Toma, M.; Zhang, Q.; Dostalek, J. Plasmon-Enhanced Fluorescence Biosensors: a Review. *Plasmonics* **2014**, *9*, 781−799.

(18) Chang, R. K., Furtak, T. E., Eds. *Surface Enhanced Raman Scattering*; Plenum Press: New York, 1982.

(19) Campion, A.; Kambhampati, P. Surface-Enhanced Raman Scattering. *Chem. Soc. Rev.* **1998**, *27*, 241−250.

(20) Haynes, C. L.; Van Duyne, R. P. Plasmon-Sampled Surface-Enhanced Raman Excitation Spectroscopy. *J. Phys. Chem. B* **2003**, *107*, 7426−7433.

(21) Hao, E.; Schatz, G. C. Electromagnetic Fields Around Silver Nanoparticles and Dimers. *J. Chem. Phys.* **2004**, *120*, 357−366.

(22) Schatz, G. C.; Young, M. A.; Van Duyne, R. P. In *Surface-Enhanced Raman Scattering: Physics and Applications*; Kneipp, K., Moskovits, M., Kneipp, H., Eds.; Springer: Berlin, 2006; pp 19−45.

(23) Stiles, P. L.; Dieringer, J. A.; Shah, N. C.; Van Duyne, R. P. Surface-Enhanced Raman Spectroscopy. *Annu. Rev. Anal. Chem.* **2008**, *1*, 601−626.

(24) Le Ru, E. C.; Etchegoin, P. G. *Principles of Surface-Enhanced Raman Spectroscopy and Related Plasmonic Effects*; Elsevier: Amsterdam, 2009.

(25) Zhang, W.; Fischer, H.; Schmid, T.; Zenobi, R.; Martin, O. J. F. Mode-Selective Surface-Enhanced Raman Spectroscopy Using Nanofabricated Plasmonic Dipole Antennas. *J. Phys. Chem. C* **2009**, *113*, 14672−14675.

(26) Margueritat, J.; Gehan, H.; Grand, J.; Lévi, G.; Aubard, J.; Félidj, N.; Bouhelier, A.; Colas des Francs, G.; Markey, L.; Lucas, C. M. D.; et al. Influence of the Number of Nanoparticles on the Enhancement Properties of Surface-Enhanced Raman Scattering Active Area: Sensitivity versus Repeatability. *ACS Nano* **2011**, *5*, 1630−1638.

(27) Trügler, A.; Tinguely, J.-C.; Jakopic, G.; Krenn, J. R.; Hohenau, A. *Phys. Rev. B: Condens. Matter Mater. Phys.* **2014**, *89*, 165409.

(28) Haes, A.; Van Duyne, R. A Unified View of Propagating and Localized Surface Plasmon Resonance Biosensors. *Anal. Bioanal. Chem.* **2004**, *379*, 920−930.

(29) Anger, P.; Bharadwaj, P.; Novotny, L. Enhancement and Quenching of Single-Molecule Fluorescence. *Phys. Rev. Lett.* **2006**, *96*, 113002.

(30) Kühn, S.; Håkanson, U.; Rogobete, L.; Sandoghdar, V. Enhancement of Single-Molecule Fluorescence Using a Gold Nanoparticle as an Optical Nanoantenna. *Phys. Rev. Lett.* **2006**, *97*, 017402.

DOI: 10.1021/acs.jpcc.6b03297
J. Phys. Chem. C 2016, 120, 21037−21046

(31) Anker, J. N.; Hall, W. P.; Lyandres, O.; Shah, N. C.; Zhao, J.; Van Duyne, R. P. Biosensing with Plasmonic Nanosensors. *Nat. Mater.* **2008**, *7*, 442−453.
(32) Camden, J. P.; Dieringer, J. A.; Wang, Y.; Masiello, D. J.; Marks, L. D.; Schatz, G. C.; Van Duyne, R. P. Probing the Structure of Single-Molecule Surface-Enhanced Raman Scattering Hot Spots. *J. Am. Chem. Soc.* **2008**, *130*, 12616−12617.
(33) Gerry, C. C.; Knight, P. L. *Introductory Quantum Optics*; Cambridge University Press: Cambridge, U.K., 2005.
(34) Purcell, E. M. Spontaneous Emission Probabilities at Radio Frequencies. *Phys. Rev.* **1946**, *69*, 681.
(35) Bian, R. X.; Dunn, R. C.; Xie, X. S.; Leung, P. T. Single Molecule Emission Characteristics in Near-Field Microscopy. *Phys. Rev. Lett.* **1995**, *75*, 4772−4775.
(36) Dulkeith, E.; Morteani, A. C.; Niedereichholz, T.; Klar, T. A.; Feldmann, J.; Levi, S. A.; van Veggel, F. C. J. M.; Reinhoudt, D. N.; Möller, M.; Gittins, D. I. Fluorescence Quenching of Dye Molecules near Gold Nanoparticles: Radiative and Nonradiative Effects. *Phys. Rev. Lett.* **2002**, *89*, 203002.
(37) Girard, C.; Martin, O. J. F.; Dereux, A. Molecular Lifetime Changes Induced by Nanometer Scale Optical Fields. *Phys. Rev. Lett.* **1995**, *75*, 3098−3101.
(38) Baffou, G.; Girard, C.; Dujardin, E.; Colas des Francs, G.; Martin, O. J. F. Molecular Quenching and Relaxation in a Plasmonic Tunable System. *Phys. Rev. B: Condens. Matter Mater. Phys.* **2008**, *77*, 121101.
(39) Kern, A. M.; Martin, O. J. F. Excitation and Reemission of Molecules near Realistic Plasmonic Nanostructures. *Nano Lett.* **2011**, *11*, 482−487.
(40) Gu, Y.; Wang, L.; Ren, P.; Zhang, J.; Zhang, T.; Martin, O. J. F.; Gong, Q. Surface-Plasmon-Induced Modification on the Spontaneous Emission Spectrum via Subwavelength-Confined Anisotropic Purcell Factor. *Nano Lett.* **2012**, *12*, 2488−2493.
(41) Yablonovitch, E. Inhibited Spontaneous Emission in Solid-State Physics and Electronics. *Phys. Rev. Lett.* **1987**, *58*, 2059−2062.
(42) Chigrin, D. N.; Lavrinenko, A. V.; Yarotsky, D. A.; Gaponenko, S. V. All-Dielectric One-Dimensional Periodic Structures for Total Omnidirectional Reflection and Partial Spontaneous Emission Control. *J. Lightwave Technol.* **1999**, *17*, 2018−2024.
(43) Lodahl, P.; Van Driel, A. F.; Nikolaev, I. S.; Irman, A.; Overgaag, K.; Vanmaekelbergh, D.; Vos, W. L. Controlling the Dynamics of Spontaneous Emission from Quantum Dots by Photonic Crystals. *Nature* **2004**, *430*, 654−657.
(44) Noda, S.; Fujita, M.; Asano, T. Spontaneous-Emission Control by Photonic Crystals and Nanocavities. *Nat. Photonics* **2007**, *1*, 449−458.
(45) Noginov, M. A.; Li, H.; Barnakov, Y. A.; Dryden, D.; Nataraj, G.; Zhu, G.; Bonner, C. E.; Mayy, M.; Jacob, Z.; Narimanov, E. E. Controlling Spontaneous Emission with Metamaterials. *Opt. Lett.* **2010**, *35*, 1863−1865.
(46) Chen, Y. P.; Sha, W. E. I.; Choy, W. C. H.; Jiang, L.; Chew, W. C. Study on Spontaneous Emission in Complex Multilayered Plasmonic System via Surface Integral Equation Approach with Layered Medium Green's Function. *Opt. Express* **2012**, *20*, 20210−20221.
(47) Härtling, T.; Reichenbach, P.; Eng, L. M. Near-Field Coupling of a Single Fluorescent Molecule and a Spherical Gold Nanoparticle. *Opt. Express* **2007**, *15*, 12806−12817.
(48) Chowdhury, M. H.; Pond, J.; Gray, S. K.; Lakowicz, J. R. Systematic Computational Study of the Effect of Silver Nanoparticle Dimers on the Coupled Emission from Nearby Fluorophores. *J. Phys. Chem. C* **2008**, *112*, 11236−11249.
(49) Liaw, J.-W.; Chen, J.-H.; Chen, C.-S.; Kuo, M.-K. Purcell Effect of Nanoshell Dimer on Single Molecule's Fluorescence. *Opt. Express* **2009**, *17*, 13532−13540.
(50) Lu, G.; Zhang, T.; Li, W.; Hou, L.; Liu, J.; Gong, Q. Single-Molecule Spontaneous Emission in the Vicinity of an Individual Gold Nanorod. *J. Phys. Chem. C* **2011**, *115*, 15822−15828.
(51) Shegai, T.; Li, Z.; Dadosh, T.; Zhang, Z.; Xu, H.; Haran, G. Managing Light Polarization via Plasmon-Molecule Interactions within an Asymmetric Metal Nanoparticle Trimer. *Proc. Natl. Acad. Sci. U. S. A.* **2008**, *105*, 16448−16453.
(52) Liaw, J.-W.; Chen, C.-S.; Chen, J.-H. Enhancement or Quenching Effect of Metallic Nanodimer on Spontaneous Emission. *J. Quant. Spectrosc. Radiat. Transfer* **2010**, *111*, 454−465.
(53) Kern, A. M.; Martin, O. J. F. Surface Integral Formulation for 3D Simulations of Plasmonic and High Permittivity Nanostructures. *J. Opt. Soc. Am. A* **2009**, *26*, 732−740.
(54) Raziman, T. V.; Somerville, W. R. C.; Martin, O. J. F.; LE RU, E. C. Accuracy of Surface Integral Equation Matrix Elements in Plasmonic Calculations. *J. Opt. Soc. Am. B* **2015**, *32*, 485−492.
(55) Johnson, P. B.; Christy, R. W. Optical Constants of the Noble Metals. *Phys. Rev. B* **1972**, *6*, 4370−4379.
(56) Oubre, C.; Nordlander, P. Optical Properties of Metallodielectric Nanostructures Calculated Using the Finite Difference Time Domain Method. *J. Phys. Chem. B* **2004**, *108*, 17740−17747.
(57) Etchegoin, P. G.; Le Ru, E. C.; Meyer, M. An Analytic Model for the Optical Properties of Gold. *J. Chem. Phys.* **2006**, *125*, 164705.
(58) Carminati, R.; Greffet, J.-J.; Henkel, C.; Vigoureux, J. Radiative and Non-Radiative Decay of a Single Molecule close to a Metallic Nanoparticle. *Opt. Commun.* **2006**, *261*, 368−375.
(59) Tai, C.-T. *Dyadic Green Functions in Electromagnetic Theory*; IEEE Press: Piscataway, NJ, 1994.
(60) Chen, S.; Liu, L.; Zhou, J.; Jiang, S. Controlling Antibody Orientation on Charged Self-Assembled Monolayers. *Langmuir* **2003**, *19*, 2859−2864.
(61) Vasilev, K.; Knoll, W.; Kreiter, M. Fluorescence Intensities of Chromophores in front of a Thin Metal Film. *J. Chem. Phys.* **2004**, *120*, 3439−3445.
(62) Ray, K.; Badugu, R.; Lakowicz, J. R. Polyelectrolyte Layer-by-Layer Assembly To Control the Distance between Fluorophores and Plasmonic Nanostructures. *Chem. Mater.* **2007**, *19*, 5902−5909.
(63) Chuang, T. J.; Eisenthal, K. B. Theory of Fluorescence Depolarization by Anisotropic Rotational Diffusion. *J. Chem. Phys.* **1972**, *57*, 5094−5097.
(64) Baffou, G.; Girard, C.; Quidant, R. Mapping Heat Origin in Plasmonic Structures. *Phys. Rev. Lett.* **2010**, *104*, 136805.
(65) Kern, A.; Martin, O. J. F. Pitfalls in the Determination of Optical Cross Sections From Surface Integral Equation Simulations. *IEEE Trans. Antennas Propag.* **2010**, *58*, 2158−2161.
(66) Jackson, J. D. *Classical Electrodynamics*, 3rd ed.; Wiley: New York, 1998.
(67) Fischer, H.; Martin, O. J. F. Engineering the Optical Response of Plasmonic Nanoantennas. *Opt. Express* **2008**, *16*, 9144−9154.
(68) Taminiau, T. H.; Stefani, F. D.; Segerink, F. B.; van Hulst, N. F. Optical Antennas Direct Single-Molecule Emission. *Nat. Photonics* **2008**, *2*, 234−237.
(69) Curto, A. G.; Volpe, G.; Taminiau, T. H.; Kreuzer, M. P.; Quidant, R.; van Hulst, N. F. Unidirectional Emission of a Quantum Dot Coupled to a Nanoantenna. *Science* **2010**, *329*, 930−933.
(70) Aouani, H.; Mahboub, O.; Bonod, N.; Devaux, E.; Popov, E.; Rigneault, H.; Ebbesen, T. W.; Wenger, J. Bright Unidirectional Fluorescence Emission of Molecules in a Nanoaperture with Plasmonic Corrugations. *Nano Lett.* **2011**, *11*, 637−644.
(71) Zhu, W.; Wang, D.; Crozier, K. B. Direct Observation of Beamed Raman Scattering. *Nano Lett.* **2012**, *12*, 6235−6243.
(72) Coenen, T.; Bernal, A. F.; Femius, K. A.; Polman, A. Directional Emission from a Single Plasmonic Scatterer. *Nat. Commun.* **2014**, *5*, 3250.
(73) Taminiau, T. H.; Stefani, F. D.; van Hulst, N. F. Enhanced Directional Excitation and Emission of Single Emitters by a Nano-Optical Yagi-Uda Antenna. *Opt. Express* **2008**, *16*, 10858−10866.
(74) Pellegrini, G.; Mazzoldi, P.; Mattei, G. Asymmetric Plasmonic Nanoshells as Subwavelength Directional Nanoantennas and Color Nanorouters: A Multipole Interference Approach. *J. Phys. Chem. C* **2012**, *116*, 21536−21546.

DOI: 10.1021/acs.jpcc.6b03297
J. Phys. Chem. C 2016, 120, 21037−21046

(75) Chew, W. C. *Waves and Fields in Inhomogenous Media*; Van Nostrand Reinhold: New York, 1990.
(76) Le Ru, E. C.; Etchegoin, P. G. Rigorous Justification of the $|E|^4$ Enhancement Factor in Surface Enhanced Raman Spectroscopy. *Chem. Phys. Lett.* **2006**, *423*, 63−66.
(77) Moskovits, M. Surface selection rules. *J. Chem. Phys.* **1982**, *77*, 4408−4416.
(78) Le Ru, E. C.; Grand, J.; Félidj, N.; Aubard, J.; Lévi, G.; Hohenau, A.; Krenn, J. R.; Blackie, E.; Etchegoin, P. G. Experimental Verification of the SERS Electromagnetic Model beyond the $|E|^4$ Approximation: Polarization Effects. *J. Phys. Chem. C* **2008**, *112*, 8117−8121.
(79) Yu, N.; Genevet, P.; Kats, M. A.; Aieta, F.; Tetienne, J.-P.; Capasso, F.; Gaburro, Z. Light Propagation with Phase Discontinuities: Generalized Laws of Reflection and Refraction. *Science* **2011**, *334*, 333−337.

DOI: 10.1021/acs.jpcc.6b03297
J. Phys. Chem. C 2016, 120, 21037−21046